Microstructure evolution in directionally solidifying Cu-17 at. %Al eutectic alloy

Małgorzata PEREK-NOWAK ⓘ*, **Grzegorz BOCZKAL** ⓘ, **Paweł PAŁKA** ⓘ, and **Piotr KUROPATWA**

Faculty of Non-Ferrous Metals, AGH University of Science and Technology, al. Mickiewicza 30, 30-059 Kraków, Poland

Abstract. An attempt of direct solidification (DS) of Cu-17 at. %Al eutectic alloy is presented in the paper. The chosen alloy belongs to the copper-rich eutectic region in the Cu–Al phase diagram. The alloy was remelted and solidified in a vertical furnace of Bridgman type with a moving crystallization zone. Thus, the expected structure will result in an arranged distribution of two phases in the bulk of the material. However, due to cooling the mentioned alloy down to room temperature, the phase transformations occur according to the respective phase diagram, including β phase decomposition through eutectoid and peritectoid reactions. The crystallized material consisted of the following phases α solution and γ_1 (Cu_9Al_4) phase. Structure observations, determination of the formed phases and texture analysis of the obtained material are described. Mechanical properties received from a tensile test are also included.

Key words: Cu–Al alloy; direct solidification; gradual material; texture.

1. INTRODUCTION

Direct solidification (DS) is a method aiming at growing elongated grains with crystallographic orientation belonging often to the same crystal zone. The method has found its application in obtaining turbine blades [1] and has been developed since then. The method facilitates producing a wide spectrum of metallic materials. The application of small velocities of crystallization zone movement together with a large temperature gradient at the crystallization front is used to obtain metal single crystals of high quality. Controlling the temperature gradient and crystallization rate is crucial in all techniques for growing single crystals like Czochralski, Bridgman [2] and zone crystallization [3–5]. Higher crystallization rates lead to achieving structures with a strong predominance of a direction. This regards directional solidification in the production of turbine blades for airplane engines or steam engines as well as studying microstructures of various transformations in many phase systems, e.g. Zn–Ti [6, 7], Zn–Ti–Cu [5, 8], Cr–Cr3Si [9], Ti–Al [10, 11], Si–TaSi2 [12, 13], NiAl–Mo [14, 15].

One of the applications of directional crystallization is gradual materials. These materials are defined by the continuous change in the structure along their length. No distinct interfaces along the growth direction are visible. By choosing crystallization conditions such as temperature gradient, heat transfer rate or movement of crystallization zone rate, it is possible to receive material with structures from a wide range of concentrations of alloying components.

The additional element, naturally associated with producing the gradual structures in direct solidification process, is segrega-

tion of elements in an alloy. It is connected primarily with segregation coefficients of the components, but also with the geometry of crystallizer [16]. In certain situations, the effect of a crucible geometry on segregation is negligible. However, in vertical furnaces, the gravitational segregation may occur, especially when elements with high difference of atomic weight are used.

The occurrence of the gradient of chemical composition at the length of the crystallized sample leads to various conditions of nucleation and growth for present phases. Hence, through the microstructural analysis of a single sample, it is possible to evaluate many variants of solidification and pre-estimate nucleation and growth conditions of individual phases and determine their crystallographic relationships [5].

The material chosen for the directional solidification experiment was Cu-17 at. %Al alloy. Hence, phase equilibria for the Cu–Al system were investigated [16, 17] paying strong attention to the Cu-rich part. The respective phase diagram [18] together with the list and crystallographic characteristics of possible phases (see Table 1 in [19]) was of obvious help. The studied alloy composition is marked on the Cu–Al phase diagram in Fig. 1.
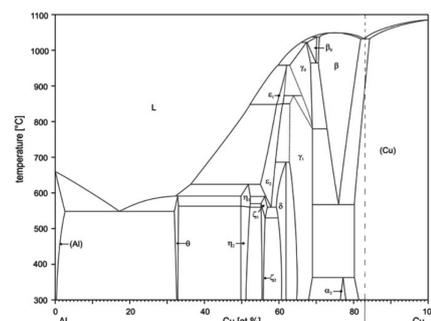

Fig. 1. Al–Cu phase diagram [18] with a marked initial concentration of DS samples (dashed line)

*e-mail: mperek@agh.edu.pl

Bull. Pol. Acad. Sci. Tech. Sci., vol. 71, no. 2, p. e144604, 2023

1

2. EXPERIMENTAL METHOD

The Cu-17 at. %Al alloy was prepared from pure metals (Cu of purity 99.99% and aluminum of purity 99.99%) by melting in a graphite crucible in a resistance furnace; the surface of the liquid alloy during the casting process was protected by borax. Then, the melt was poured into a graphite crucible designed for a direct solidification experiment. The crucible had a shape of a cylinder (Fig. 2). It consisted of a main chamber and a wider ingot part, where an excess of the poured alloy may remain. The main chamber was sharpened at the bottom to provide the formation of a first primary crystal as a crystallization embryo. The growth process has begun from this crystallization of the first nucleus and moved up along the main chamber together with the raising of the furnace. The main chamber had a square cross-section of 5×5 mm and a length of 100 mm.
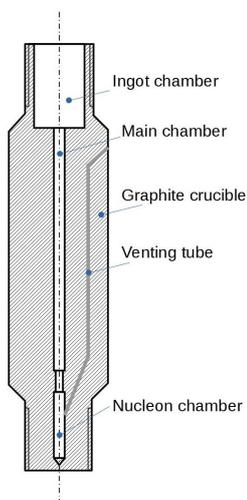

Fig. 2. Schematic illustration of a crucible used in the experiment

Fig. 3. Furnace for directional solidification a) schematic diagram, b) image of real equipment

The furnace for directional solidification was designed as Bridgman type, presented in Fig. 3. There was a quartz tube inside into which a graphite crucible was inserted. The length of a quartz tube was 600 mm. The furnace moved along the tube from bottom to top at a rate of 18 mm/h. It is noteworthy that before heating the gases from the quartz tube were evacuated by a vacuum pump and argon N5 gas was introduced. Thus, it was ensured that the remelting of the alloy occurred in a protective atmosphere.

The material obtained in the Bridgman process had a form of a $5 \times 5 \times 100$ mm prism. In a cursory inspection of the light microscope, there were visible three regions of different arrangements of peritectoid microstructure along the growth direction (GD). Therefore, the DS bar was cut and three samples representative of each region were extracted (as presented in Fig. 4).

Next, the phase identification was carried out by X-ray powder diffraction method for each of the three samples. Besides, for each region, the texture was obtained for the phases determined by powder diffraction. The XRD analyses, both powder and texture diffractions, were performed with the use of Bruker D-8 Advance diffractometer with Cu tube. The texture measurements (pole figures) were recalculated in the MTEX tool-
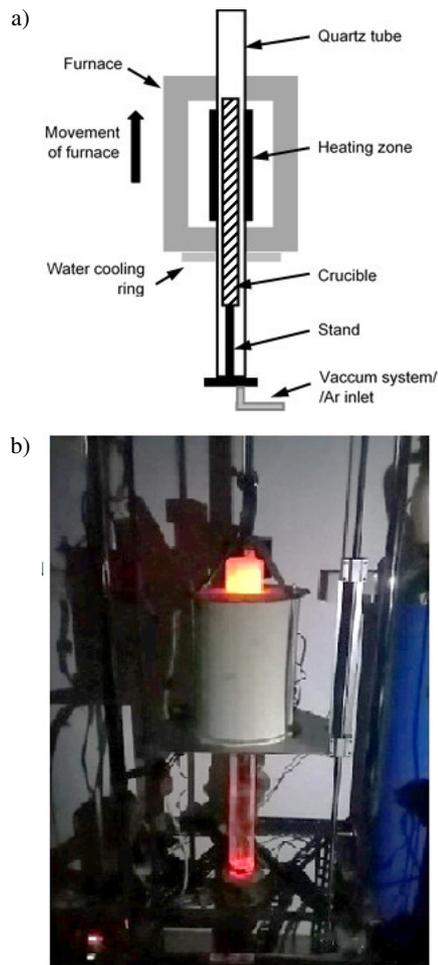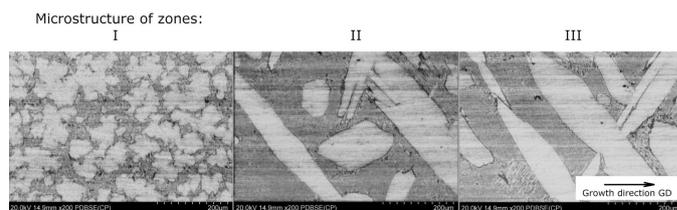

Fig. 4. Schematic representation of three characteristic regions in order of growth sequence, from which samples were taken

box for Matlab [20] to obtain pole figures (PF) and orientation distribution function (ODF).

The samples characteristic for each region (smaller pieces in Fig. 3) were observed by means of scanning electron microscopy (SEM) where backscattered electron (BSE) contrast was of special use as it allowed us to distinguish between two Cu–Al phases. Additionally, X-ray energy dispersion spectrometry (EDS) analyses were made to establish regions richer in Cu or Al. The observations were done at SEM Hitachi S-3400N at an accelerating voltage of 20 kV and a working distance of 5 mm and 11 mm for EDS. The EDS attachment was produced by Thermo Noran.

Finally, samples for tensile tests were cut out by means of an electro-erosion wire saw from the larger portions of the DS rod presented in Fig. 4. The dimension of the samples was the following: cross-section of 2×2.5 mm and length of 12 mm. The samples were cut along the growth direction GD. The tensile characteristics were collected at room temperature at Instron 5566 machine up to rupture. The applied strain rate during deformation was 10^{-3} s^{-1}.

3. EXPERIMENTAL RESULTS AND DISCUSSION

During crystallization, theoretically, one nucleus should be formed which would propagate through the crucible. However, in the situation described in the article, there are either few embryos formed at the beginning of solidification, or significant fluctuations at the crystallization front arise. The fluctuations may be caused by the crystallization of two phases from the liquid and may be a reason for the formation of other grains.

The obtained bars after DS growth were characterized with respect to the phases present. The material was composed to analyze the processes occurring during the crystallization of a copper-rich eutectic alloy. As it can be read from the Cu–Al phase diagram (Fig. 1), during cooling the Cu-17 at. %Al alloy down to room temperature another transformation takes place. The eutectic phase β decomposes to γ_1 phase and α at the eutectoid point according to a reaction: $\beta \rightarrow \gamma_1 + \alpha$ (at a temperature of 567°C). There is also a peritectoid reaction, in which the α_2 phase may be formed. Taking a closer look at a phase diagram in Fig. 1 and the possible phases listed in [19] we realize, that it might be difficult to find the α_2 phase as it is a long-period superlattice FCC structure [19] (similar to the α phase, also FCC) and differs by only 2 at. % to a maximum of 3.8 at. % from the α phase [19]. The powder diffraction does not show any signs of α_2 either (Fig. 5). According to a recent description of phases formation in the Cu–Al system by Liang [19], the chemical composition of the γ_1 phase is Cu_9Al_4 crystallizing in $P\bar{4}3m$ space group while α is a solid solution with $Fm\bar{3}m$ (FCC) crystal lattice [19]. The arrangement of atoms in $Cu_9Al_4 \gamma$ brasses is thoroughly described and visualized in [21].

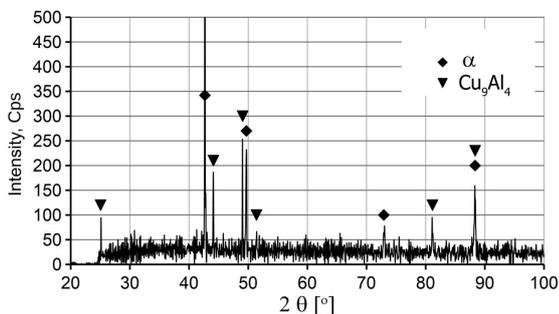**Fig. 5.** Powder diffraction spectrum defining phases present in the material, Cu–Al solid solution α and γ_1 phase (Cu_9Al_4)

Therefore, to identify the phases that could have been formed during solidification, the powder diffraction measurement was carried out. The result (Fig. 5) confirms indeed the presence of solid solution α and the γ_1 phase.

3.1. Microstructure observations

With known phases present in the alloy, the microstructure of the samples was evaluated by means of scanning electron microscopy (SEM). The characteristic arrangement of the phases for each region of the DS bar is presented in Figs. 6–8. Sample 1 that resolidified at first is composed of equiaxed regions of solid solution surrounded by a eutectoid structure. The second region is characterized by larger areas of solid solution α but less densely distributed within the bar. The most interesting is the third portion of the material, where the α phase takes a lenticular form within the surrounding α/γ_1 eutectoid.

Interestingly, in images collected at higher magnifications of $500\times$ and $5000\times$ (Figs. 6–8), an outer envelope of the γ_1 phase is present. The thickness of this halo is up to 3 μm.
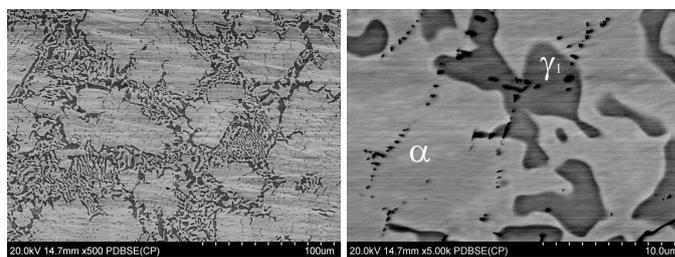

Fig. 6. Microstructure of a sample taken from zone I of DS rod; SEM observed using BSE detector; magnifications $500\times$ and $5000\times$
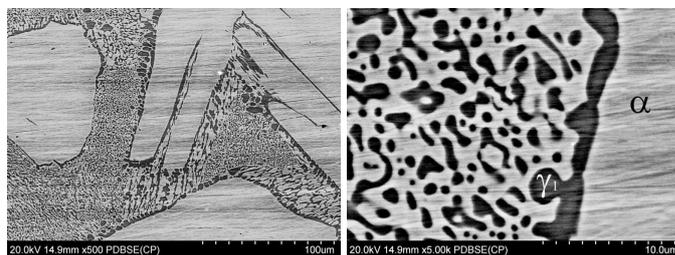

Fig. 7. Microstructure of a sample taken from zone II of DS rod; SEM observed using BSE detector; magnifications $500\times$ and $5000\times$
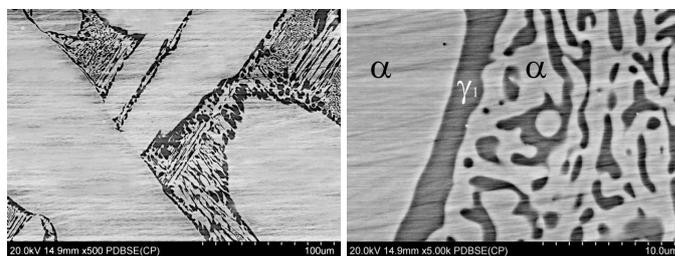

Fig. 8. Microstructure of a sample taken from zone III of DS rod; SEM observed using BSE detector; magnifications $500\times$ and $5000\times$

As it was stated previously, the α phase takes a lenticular form within the surrounding α/γ_1 eutectoid. It is to note, that the lenticular regions are placed quite parallel (Fig. 9) within the sample. Besides, another family of lenses is also visible in the image with an apparent axis rotated about 70° (lines in

Bull. Pol. Acad. Sci. Tech. Sci., vol. 71, no. 2, p. e144604, 2023

3

Fig. 9). It can be assumed that the elliptical-like structures localized with the longer axis along the growth direction are also lens-shaped α phase but oriented in such a way that the surface of the sample intersects them (the cross-section of the lens is visible). It can be imagined that the α phase is formed along three directions in the structure forming a kind of woven construction in the material.
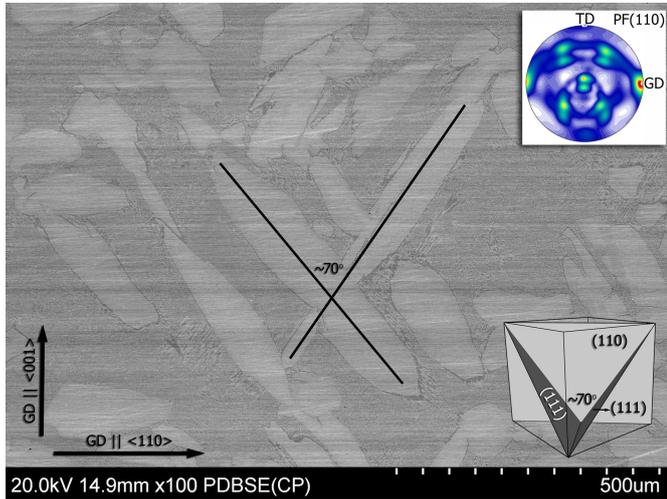

Fig. 9. Microstructure with ordered precipitations of a phase. Angular relation was marked on the unit cell and pole figure

The inset in Fig. 9 explains that the massive precipitates of α phase grow on the $\{111\}$ planes. The angle between planes belonging to that family is $70.5°$. It is also marked that the plane of observation is (110) plane and the growth direction, GD, of the rod is parallel to $\langle 110 \rangle$.

The attached $\{110\}$ pole figures (Fig. 9) are aligned with GD oriented as it is in the image. The pole figures will be discussed further in Section 3.3.

Additionally, EDS analysis was made in microregions of zone II (Fig. 10) to determine regions richer in copper or aluminum. The established composition in the marked points is given in Table 1. It is noted that brighter regions are solid solution α (points 1 and 3), indeed, while the darker ones (points 2 and 4) belong to the γ phase.

Table 1
Chemical composition in the points marked in Fig. 9 in at.%

Measurement point	Al–K	Cu–K
pt1	19.92	80.08
pt2	30.83	69.17
pt3	20.46	79.54
pt4	29.39	70.61

3.2. Mechanical properties

Samples representing three regions of the DS bar were deformed in a tensile test with a strain rate of 10^{-3} s^{-1} (Fig. 11)
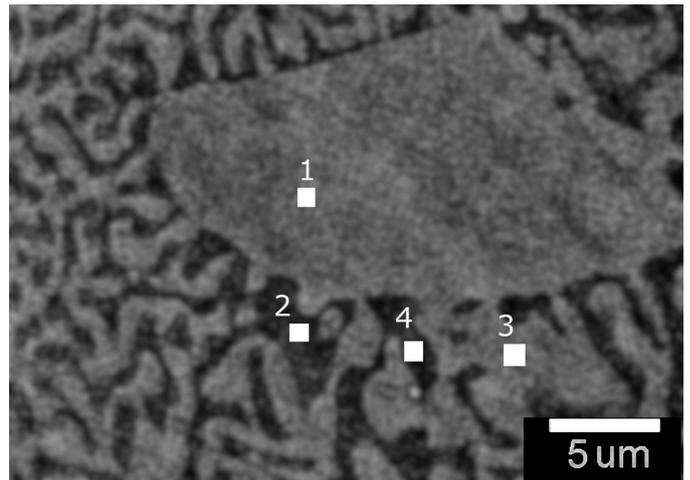

Fig. 10. EDS analysis in microregions

at Instron 5566 tensile machine. All samples exhibited a brittle type of deformation with a true strain below 0.1. However, the ultimate tensile strength is quite high in the range from 490 MPa up to 630 MPa. After achieving the mentioned levels of stress, a sudden rupture followed. It appears that the sample extracted from the region that resolidified first (sample 1) and characterized by the microstructure of equiaxed regions of solid solution surrounded by the eutectoid structure (Fig. 6) shows the highest strength (630 MPa). On the other hand, the sample belonging to the middle region of the DS bar (sample 2) with large regions of solid solution surrounded by Cu–Al eutectoid (Fig. 7) has the lowest strength of only 490 MPa. Interestingly, the sample from the last portion of the DS bar (sample 3) with well-developed lenticular α regions (Fig. 8) has again high tensile strength of 550 MPa.
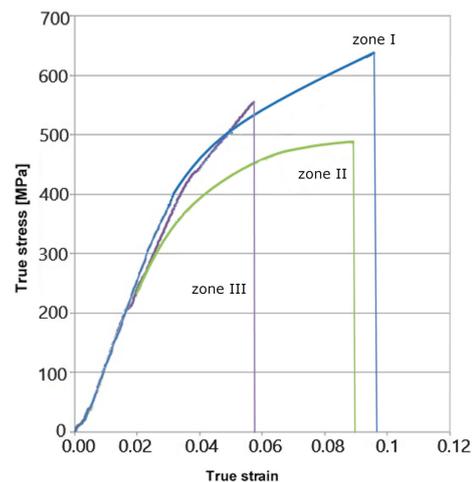

Fig. 11. Tensile characteristic of samples belonging to three zones of a DS rod

3.3. Texture observations

Since it was established, there have been two phases in the volume of the DS material: α and γ_1 (see Fig. 5), the texture was measured in a form of pole figures (PF) for both of the phases.

4

Bull. Pol. Acad. Sci. Tech. Sci., vol. 71, no. 2, p. e144604, 2023

The texture was collected at three crystallographic planes for each of the lattices: {100}, {110}, {111} for α phase, and {001}, {330}, {111} for γ_1 phase. It is noteworthy that the growth direction of phase α is parallel to $\langle 110 \rangle$ direction. On the other hand, the γ_1 phase grows along a direction $10°$ apart from $\langle 100 \rangle$.

Additionally, Figs. 12 and 13 present the distribution of poles of the chosen planes for the measurement. It appears that during crystallization, the poles of the α phase arrange themselves at similar planes separated by about $18°$ distance (see Fig. 12b). This means that the grains have orientation being in a crystallographic dependence and belonging to one crystallographic zone. On the other hand, the γ_1 phase represents a strong cubic component ({110} poles) with {330} poles lying at large circles (Fig. 14). Besides, {111} poles suggest that the γ phase grows in twin orientation in the DS rod.
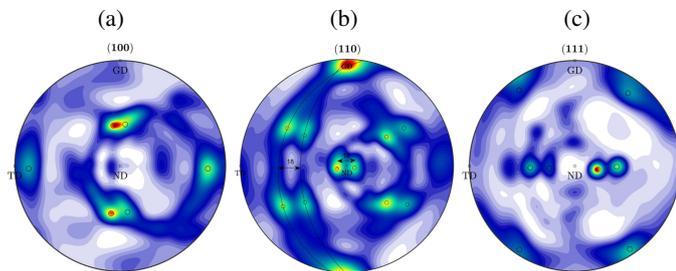

Fig. 12. Pole figures of sample from zone 3 of DS rod measured for α phase at three crystallographic planes {100}, {110}, {111} and re-calculated in MTEX toolbox for Matlab
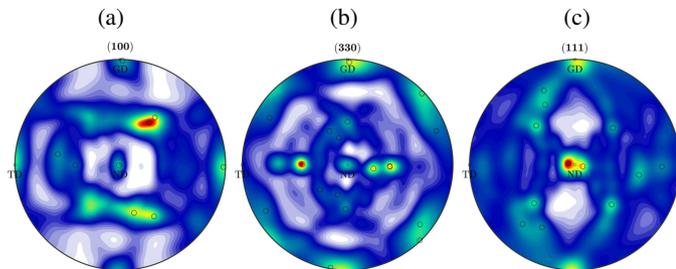

Fig. 13. Pole figures of sample from zone 3 of DS rod measured for γ_1 phase at three crystallographic planes {100}, {330}, {111} and re-calculated in MTEX toolbox for Matlab

The data collected during PF measurement was also used to calculate an ODF in MTEX (Figs. 14 and 15). The arrangement of a fiber confirms that the grain orientations in the sample are in crystallographic relations (Fig. 14).

Two main texture components for the α phase were determined using MTEX. These components are distinguished by a common $\langle 110 \rangle$ pole parallel to GD and [–110] direction parallel to ND with a considerable spread of about $18°$. The components are marked in Fig. 12 with circles.

The γ_1 phase can be described with three components: first, close to cubic orientation, second and third with $\langle 110 \rangle$ pole parallel to GD and (111) plane parallel to ND are present in a mutual symmetrical correlation with habitus plane parallel to ND.
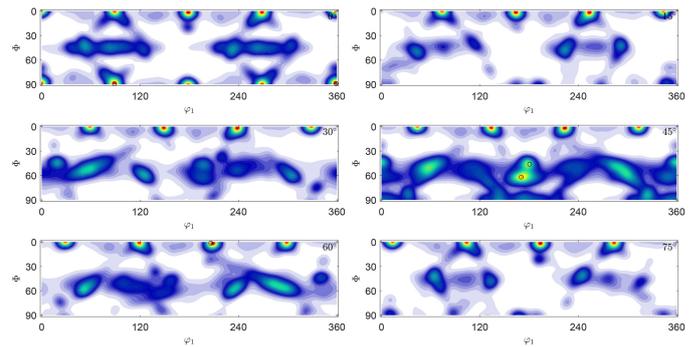

Fig. 14. ODF representation of orientation measured for α phase in a sample from zone 3 of DS rod; it corresponds to Fig. 12
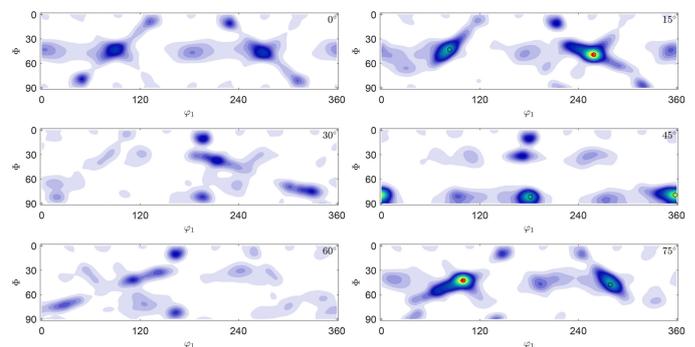

Fig. 15. ODF representation of orientation measured for γ_1 phase in a sample from zone 3 of DS rod; it corresponds to Fig. 13

Analysis of an orientation distribution function (ODF) showed that all three texture components for the γ_1 phase are always present in a constant angular correlation of about 45 degrees to Goss texture.

The analysis of PFs and ODFs points to a strong dependence of α and γ_1 phases on the common growth direction GD parallel to $\langle 110 \rangle$. It is noteworthy that the ND of the α phase, which is parallel to the (110) plane, is also parallel to the (111) plane in the γ phase.

4. SUMMARY

The Cu–Al rods with gradual structure were produced in direct solidification process. Their microstructure consisted in α and γ_1 phases which were detected with XRD and SEM/EDS analyses. The mechanical tests showed high strength levels with low elongation while fractures were brittle in character. The texture measurements presented in PFs and ODFs show mutual crystallographic dependence between the grown phases. Besides, the observed grains belong to one crystallographic zone, thus their orientation cannot significantly differ.

ACKNOWLEDGEMENTS

REFERENCES

[1] F.L. Ver Snyder, R.W. Guard, "Directional grain structure for high temperature strength," *Trans. ASM*, vol. 52, pp. 485–492, 1960.

[2] M. Philippov *et al*, "Modeling of dynamics of big size ZnGeP2 crystal growth by vertical Bridgman technique," *Bull. Pol. Acad. Sci. Tech. Sci.*, vol. 66, pp. 283–290, 2018, doi: 10.24425/123434.

[3] H.J. Scheel, "Historical aspects of crystal growth technology," *J. Cryst. Growth*, vol. 211, pp. 1–12, 2000, doi: 10.1016/S0022-0248(99)00780-0.

[4] A.J. Clarke *et al.*, "Microstructure selection in thin-sample directional solidification of an Al-Cu alloy: In situ X-ray imaging and phase-field simulations," *Acta Mater.*, vol. 129, pp. 203–216, 2017, doi: 10.1016/j.actamat.2017.02.047.

[5] G. Boczkal, "Second phase morphology in the Zn-Ti0.1-Cu0.1 single crystals obtained at different growth rates," *Arch. Met. Mater.*, vol. 57, pp. 479484, 2012, doi: 10.2478/v10172-012-0049-9.

[6] G. Boczkal, B. Mikułowski, I. Hünsche, C.-G. Oertel, and W. Skrotzki, "Precipitation of intermetallic phase in Zn–Ti alloy single crystals," *Cryst. Res. Technol.*, vol. 43, pp. 135–140, 2008, doi: 10.1002/crat.200711068.

[7] G. Boczkal, B. Mikułowski, C.-G. Oertel, and W. Skrotzki, "Work-hardening characteristics of Zn–Ti alloy single crystals," *Cryst. Res. Technol.*, vol. 45, pp. 111–114, 2010, doi: 10.1002/crat.200900537.

[8] G. Boczkal, "Structure and properties of Zn–Ti0.2–Cu0.15 single crystal containing eutectic precipitates," *Arch. Met. Mater.*, vol. 58, pp. 1019–1022, 2013, doi: 10.2478/amm-2013-0020.

[9] H. Bei, E.P. George, E.A. Kenik, and G.M. Pharr, "Directional solidification and microstructures of near-eutectic Cr-Cr3Si alloys," *Acta Mater.*, vol. 51, pp. 6241–6252, 2003, doi: 10.1016/S1359-6454(03)00447-6.

[10] S.E. Kim, Y.T. Lee, M.H. Oh, H. Inui, and M. Yamaguchi, "Directional solidifcation of TiAl-Si alloys using apolycrystalline seed," *Intermetallics*, vol. 8, pp. 399–405, 2000, doi: 10.1016/S0966-9795(99)00122-3.

[11] M. Yamaguchi, D.R. Johnson, H.N. Lee, H. Inui, "Directional solidifcation of TiAl-base alloys," *Intermetallics*, vol. 8, pp. 511–517, 2000, doi: 10.1016/S0966-9795(99)00157-0.

[12] C. Cui, J. Zhang, B. Li, M. Han, L. Liu, and H. Fu, "The preferential orientation of the directionally solidified Si–TaSi2 eutectic in situ composite," *J. Cryst. Growth*, vol. 309, pp. 93–96, 2007, doi: 10.1016/j.jcrysgro.2007.09.001.

[13] C. Cui, J. Zhang, H. Su, L. Liu, and H. Fu, "Growth mechanism of the directionally solidified Si–TaSi2 eutectic in situ composite," *J. Cryst. Growth*, vol. 311, pp. 2555–2559, 2009, doi: 10.1016/j.jcrysgro.2009.02.014.

[14] H. Bei and E.P. George, "Microstructures and mechanical properties of a directionally solidified NiAl–Mo eutectic alloy," *Acta Mater.*, vol. 53, pp. 69–77, 2005, doi: 10.1016/j.actamat.2004.09.003.

[15] P. Ferrandini, W.W. Batista, and R. Caram, "Influence of growth rate on the microstructure and mechanical behaviour of a NiAl–Mo eutectic alloy," *J. Alloy. Compd.*, vol. 381, pp. 91–98, 2004, doi: 10.1016/j.jallcom.2004.02.052.

[16] M. Gündüz and E. Çadırlı, "Directional solidification of aluminium–copper alloys," *Mater. Sci. Eng. A*, vol. 327, pp. 167–185, 2002, doi: 10.1016/S0921-5093(01)01649-5.

[17] X.J. Liu, I. Ohnuma, R. Kainuma, and K. Ishida, "Phase equilibria in the Cu-rich portion of the Cu–Al binary system," *J. Alloy. Compd.*, vol. 264, pp. 201–208, 1998, doi: 10.1016/S0925-8388(97)00235-1.

[18] T.B. Massalski, J.L. Murray, L.H. Bennet, and H. Baker, *Binary Alloy Phase Diagrams*. Metals Park OH: American Society for Metals, 1986.

[19] S.M. Liang and R. Schmid-Fetzer, "Thermodynamic assessment of the Al–Cu–Zn system, part II: Al–Cu binary system," *Calphad*, vol. 51, pp. 252–260, 2015, doi: 10.1016/j.calphad.2015.10.004.

[20] R. Hielscher and H. Schaeben, "A novel pole figure inversion method: specification of the MTEX algorithm," *J. Appl. Crystallogr.*, vol. 41, pp. 1024–1037, 2008, doi: 10.1107/S0021889808030112.

[21] U. Mizutani, M. Inukai, H. Sato, and E.S. Zijlstra, *Electron Theory of Complex Metallic Alloys, in Physical Metallurgy*. D.A. Laughlin, K. Hono, Eds., vol. 1, 5th ed., Elsevier: Amsterdam, 2014, pp. 103–200, doi: 10.1016/B978-0-444-53770-6.00002-2

6

Bull. Pol. Acad. Sci. Tech. Sci., vol. 71, no. 2, p. e144604, 2023